Brain Connectivity

DOI: 10.1089/brain.2022.0047


# Correlative chemical imaging identifies amyloid peptide signatures of neuritic plaques and dystrophy in human sporadic Alzheimer's disease

Srinivas Koutarapu[1], Junyue Ge[1], Durga Jha [1,2], Kaj Blennow [1,3], Henrik Zetterberg [1,3,4,5,6], Tammaryn Lashley [4,7], Wojciech Michno [1,8,9] and Jörg Hanrieder [1,4]*

1) Department of Psychiatry and Neurochemistry, Sahlgrenska Academy, University of Gothenburg, Mölndal, Sweden

2) Masaryk University, Brno, Czech Republic

3) Clinical Neurochemistry Laboratory, Sahlgrenska University Hospital, Mölndal, Sweden

4) Department of Neurodegenerative Disease, Institute of Neurology, University College London, London, United Kingdom

5) UK Dementia Research Institute, University College London, London, United Kingdom

6) Hong Kong Center for Neurodegenerative Diseases, Hong Kong, China

7) Queen Square Brain Bank for Neurological Disorders, Department of Clinical and Movement Neurosciences, Queen Square Institute of Neurology, University College London, London, United Kingdom

8) Department of Neuroscience, Physiology and Pharmacology; University College London, London, United Kingdom

9) Department of Pediatrics, Stanford University School of Medicine, Stanford University

Contact:

*Jörg Hanrieder, PhD

Department of Psychiatry and Neurochemistry, Sahlgrenska Academy, University of Gothenburg, Mölndal, Sweden

jh@gu.se; Phone +46-31-3732344

**ABSTRACT**

**Objective:** Alzheimer's disease (AD) is the most common neurodegenerative disease. The predominantly sporadic form of AD (sAD) is age-related, but the underlying pathogenic mechanisms remain not fully understood. Current efforts to combat the disease focus on the main pathological hallmarks, in particular beta-amyloid (Aβ) plaque pathology. According to the amyloid cascade hypothesis, Aβ is the critical early initiator of AD pathogenesis. Plaque pathology is very heterogeneous, where a subset of plaques, neuritic plaques, are considered most neurotoxic rendering their in depth characterization essential to understand Aβ pathogenicity. **Methods:** To delineate the chemical traits specific to neuritic plaque types, we investigated senile Aβ pathology in post mortem human sporadic AD brain using advanced correlative biochemical imaging based on immunofluorescence microscopy and mass spectrometry imaging (MSI).

**Results:** Immunostaining-guided MSI identified distinct Aβ signatures of neuritic plaques characterized by increased Aβ 1-42(ox) and Aβ2-42. Moreover, correlation with a marker of dystrophy (reticulon 3, RTN3) identified key Aβ species that both delineate neuritic plaques and display association with neuritic dystrophy.

**Conclusion:** Together these correlative imaging data shed light on the complex biochemical architecture of neuritic plaques and associated dystrophic neurites. These in turn are obvious targets for disease-modifying treatment strategies, as well as novel biomarkers of Aβ pathogenicity.

**Impact statement**

Using advanced biochemical imaging tools, we delineate Aβ signatures associated with neurotoxic plaque pathology in postmortem human brain. The results implicate N-terminal Aβ processing and oxidative stress to be key in Aβ pathogenicity and neurotoxicity. These data highlight the great potential of mass spectrometry imaging to shed light on specific biochemically heterogenous plaque morphologies, which cannot be delineated with conventional staining approaches. The distinct molecular traits identified for neuritic plaque pathology are in turn obvious targets for disease-modifying treatments, as well as potential novel biomarkers of Aβ pathogenicity.

**Keywords**: Matrix assisted laser/desorption ionization mass spectrometry imaging (MALDI MSI), Alzheimer's disease (AD), beta amyloid, neuritic plaques, cored plaques, dystrophic neurites

**Abbreviations.** AD, Alzheimer's disease; Aβ, beta-amyloid; IF, Immunofluroscence; LCO, Luminescent Conjugated Oligothiophenes; MSI, Mass Spectrometry Imaging; PHF Paired helical filament; NFT, Neurofibrillary tangles; RTN3, Reticulon-3; ROI region of Interest

## INTRODUCTION

Alzheimer's disease (AD) is the most common neurodegenerative disorder affecting nearly 12% of individuals older than 65 years (Matthews et al., 2019). The disease poses an immense societal challenge and personal suffering, particularly as there are still no curative treatments as the pathogenic mechanisms of AD remain elusive (Matthews et al., 2019). Impaired memory is the earliest clinical symptom of AD but the disease does not manifest as severe dementia until the late stage of disease (Selkoe, 2002). The formation of extracellular amyloid-beta (Aβ) plaques and hyper-phosphorylated tau in neurofibrillary tangles (NFT) (Braak and Braak, 1991) in the brain are pathological hallmarks of AD. The prevailing model of AD pathogenesis is that the changes in Aβ metabolism precipitate a damaging cascade upstream of tau pathology and eventual neurodegeneration. Here, diversity of Aβ aggregates, linked to Aβ peptide species, is considered an important driver of pathological changes. This component of AD pathology however is still poorly characterized. Nevertheless, the relevance of Aβ, and particularly its aggregates in AD, has seen a recent resurgence following the FDA approval of aducanumab, a monoclonal antibody targeting aggregated Aβ (Sevigny et al., 2016). There are also several submissions for accelerated approval of additional biologics, e.g., lecanemab and donanemab. Lecanemab reduces Aβ deposition by binding to the protofibrils of Aβ (Swanson et al., 2021) and donanemab interacts with pyroglutamated aggregates present in the core of the plaques and prevents growth of the plaques (Bayer, 2022). On the diagnostic side, a blood test for diagnosing AD by measuring Aβ isoforms was recently approved by the FDA (PrecivityAD, (Kirmess et al., 2021)).

Extracellular Aβ plaques constitute a highly heterogeneous population that are commonly annotated as thioflavin (Th) or Congo red (CR)-positive cored plaques and conversely Th/CR-negative diffuse plaques. Moreover, a subset Th-positive plaques includes neuritic plaques (NP) that are characterized by the presence of neurites. These neurites are composed of pre-helical tau protein filaments and hyperphosphorylation of these tau filaments is one of the earliest cytoskeletal changes observed in the neurites associated with NPs (Su *et al.* 1996). Biochemically, these neurites and NPs, respectively, can be delineated using an anti-PHF-1 antibody that recognizes Tau species doubly

Brain Connectivity
Correlative chemical imaging identifies amyloid peptide signatures of neuritic plaques and dystrophy in human sporadic Alzheimer's disease (DOI: 10.1089/brain.2022.0047)
This paper has been peer-reviewed and accepted for publication, but has yet to undergo copyediting and proof correction. The final published version may differ from this proof.

phosphorylated at $Ser^{396}$ and $Ser^{404}$ (Otvos et al., 1994). Further, NPs are found to be associated with neuronal aberrations, dystrophic neurites that are abnormal neuritic sproutings, swollen dendrites and/or axons scattered throughout the grey matter in AD brain and their presence and prevalence was found to correlate with synaptic degradation (Shi et al., 2009). DNs are both associates with amyloid plaque pathology (i.e. NPs) but show localizations unaffiliated with amyloid deposits (Dickson et al., 1999, Lenders et al., 1989) Histochemical, immunohistochemical and electron microscopy analyses of plaque associated dystrophic neurites showed that those structures contain many proteins, including synaptic and axonal proteins such as phosphorylated Tau, APP, neurofilaments, ubiquitin, pentraxins and reticulon (Lenders et al., 1989, Sharoar et al., 2019). Specifically, reticulon 3 (RTN3) is an abundant constituent of tubular endoplasmic reticulum (ER) and consequently, abundant levels of RTN3 are released during ER degradation (Grumati et al., 2017) such as in dystrophia. Interestingly, RTN3 has been demonstrated to label an abundant population of DNs in AD brains that was associated with cognitive decline (Shi et al., 2009), and most importantly association of RTN3-immunopositive dystrophic neurites (RIDN) was found to be associated with NPs but was not witnessed around other plaque types (Hu et al., 2007). Together PHF and RTN3 have been demonstrated to be robust tools to differently outline NPs among complex and heterogenous amyloid plaque pathology in postmortem human AD brain tissue. Given the association of NP and the associated DN's with synaptic and neuronal degeneration further biochemical characterization of NP types are of great relevance. More so, characterizing the Aβ makeup of NPs could be critical important to further understand the relation of Aβ pathology and neurodegenerative downstream processes. In addition, those NP specific Aβ signatures are obvious dug targets and can further serve as fluid biomarkers indicative of neuritic plaque pathology and Aβ pathogenicity. In situ characterization of Aβ isoforms is challenging when using conventional immuno-based methods. These challenges are overcome with the advent of matrix assisted laser desorption ionization (MALDI) based MSI, which is an emerging powerful biochemical imaging technology well suited for in situ Aβ peptide analysis at the single plaque level (Hanrieder et al., 2011, Michno et al., 2019a, Michno et al., 2021, Michno et al., 2020, Michno et al., 2019b).

In this study, we set out to interrogate the differences of neuritic and non-neuritic cored plaques in post mortem human sAD brain. For this we devised a correlative chemical imaging strategy comprising fluorescent amyloid staining luminescent oligothiophenes (LCO; qFTAA and hFTAA) along with markers of neuritic plaques (PHF-1) (Dickson and Vickers, 2001, Moloney et al., 2021) and dystrophic neurites (RTN3) (Shi et al., 2009). The correlative IHC/amyloid signatures were used together to guide subsequent mass spectrometry imaging (MSI) analysis on the facing surface of the consecutive (i.e.sequential) tissue section (mirror section) to determine the associated Aβ signatures of those individual plaque types.

Together, the correlative LCO/IHC and MALDI MS imaging revealed increased levels of Aβ1-42(ox) and Aβ2-42 in neuritic (PHF+) as compared to non-neuritic (PHF-) cored plaques.

## MATERIALS AND METHODS

### Chemicals and Reagents

All chemicals for matrix and solvent preparation were pro-analysis grade and obtained from Sigma-Aldrich/Merck (St. Louis, MO), unless otherwise specified. TissueTek optimal cutting temperature (OCT) compound was purchased from Sakura Finetek (Cat.#: 4583, AJ Alphen aan den Rijn, The Netherlands). Deionized water was obtained by a Milli-Q purification system (Millipore Corporation, Merck, Darmstadt, Germany).

### Patient Samples

Fresh brain tissue samples were obtained from the superior temporal cortex of 3 clinically and pathologically diagnosed sAD patients (Table 1). All cases were obtained through the brain donation program of the Queen Square Brain Bank for Neurological Disorders (QSBB), Department of Clinical and Movement Neurosciences, UCL Queen Square Institute of Neurology. The standard diagnostic criteria were used for the neuropathological diagnosis of AD (Montine et al., 2012). Ethical approval for the study was obtained from the Local Research Ethics Committee of the National Hospital for Neurology and Neurosurgery as well as the Institutional Review Board at the University of Gothenburg

(Gothenburg, 04/16/2015; DNr 012-15). All studies abide by the principles of the Declaration of Helsinki.



Brain Connectivity
Correlative chemical imaging identifies amyloid peptide signatures of neuritic plaques and dystrophy in human sporadic Alzheimer's disease (DOI: 10.1089/brain.2022.0047)



**Sample Preparation**

Sequential tissue sections (12µm) were collected on a cryostat microtome (Leica CM1900, Leica Biosystems, Nussloch, Germany) as a set of mirror sections i.e. with the facing surfaces of two sequential sections placed upwards on individual glasses for the respective, orthogonal imaging experiments (IF vs MSI). The operating temperature of the cryostat was maintained at -18$^{o}$C to -20$^{o}$C. Utmost care was taken to avoid the interference of the OCT mounting media while sectioning the brain tissues. These mirror sections provide access to the two closest possible surfaces. One of the mirror sections is thaw mounted on to the super frost slides for fluorescent microscopy while the other onto the charged surface of the indium tin oxide (ITO)-coated, conductive glass slides (Cat. #: 237001, Bruker Daltonics GmbH & Co. KG, Bremen, Germany) for MALDI imaging. Brain sections from all the patients included in the study are collected in a similar operating conditions. All samples were stored at -80°C until further use. Prior to matrix deposition, samples were thawed in a desiccator under reduced pressure for 30 min.

**Immunohistochemistry**

For immunohistochemistry and fluorescent amyloid imaging, sections on superfrost glasses were fixed in gradient concentration of ice cold 95%, 70% ethanol and 1xPBS at room temperature. Sections were then blocked with (Bovine Serum Albumin BSA, Normal Goat Serum NGS, Triton in 0.1% PBST) for a period of 90 minutes at room temperature. The sections were then incubated with cocktail of two primary antibodies PHF-1 (Courtesy of Dr. Peter Davies, Feinstein Institute for Medical Research) and RTN3 (Cat. No. ABN1723) diluted in PBS-T with 0.2% NGS (PHF-1: 1:500 and RTN3: 1:1000) for over 18 hours at 4$^{o}$C. Sections were washed with 0.1% PBST and incubated with secondary antibodies (Alexa-fluor594 Catalog # A32740; Alexa-fluor 647- Catalog # A32728) for a duration of 60 min at room temperature. All the brain sections were then treated with autofluorescence quenching agent Trueblack™ 1X for 30 sec and are later subjected to three PBS washes of 5 minutes each. To stain amyloid and tau morphologies, antibody-stained sections were

incubated with two previously validated LCO fluorophores ( tetrameric formyl thiophene acetic acid ,q-FTAA, 2.4 µM in MilliQ water) and heptameric formyl thiophene acetic acid (h-FTAA, 0.77 µM in MilliQ water), in the dark for 25 min. Subsequently, the sections were subjected to a single 10 min 1x PBS wash followed by mounting with DAKO fluorescent mounting media and incubated in the dark for 24 hours until further imaging.

**Fluorescent Microscopy**

The multichannel imaging of immuno-stained human brain sections was performed using an automatic widefield microscope (Axio Observer Z1, Zeiss, Germany). Large multi-channel tile scans were captured using EGFP, Alexafluor594 and Alexafluor647 filter sets. All the images were captured using Plan-Apochromat 20×/0.8 DIC air objective lens. The acquisition settings were adjusted to prevent saturation or bleed through during the acquisition of multichannel images acquired with EGFP/Alexafluor594 / Alexafluor647 filter sets.

**Image Analysis**

FIJI Image J was used for post processing of images. Here, files from each channel were split into gray scale images and are subjected to background subtraction. Here EGFP/Green channel with LCO stained plaques are used as a reference image for marking the regions occupied by plaques. Segmentation was performed on Green channel using Li threshold method. Wand tool iwas used to mark the segmentation and are saved to ROI manager. These ROI annotations are used to acquire intensity measurement from the corresponding gray scale image of anti PHF-1/Red channel and anti RTN3/Blue channel. Fluorescence intensities was calculated as intensity/$\mu m^2$.

All amyloid plaques were identified based on the LCO fluorescent signal (LOC+) and further divided into two groups based on the immunoreactivity towards PHF-1. If a plaque showed positive immunoreactivity for PHF-1, then the plaque was referred to as PHF+/neuritic or else was referred to as PHF-/non-neuritic. Further, all LCO+ plaques were investigated for RTN3 immunoreactive dystrophic neurites (RINDs). Here only LCO+/PHF+ plaques showed presence of RINDs.

**MALDI MSI Sample Preparation**

For amyloid peptide imaging, we employed a previously validated protocol for robust peptide and protein mass spectrometry imaging (Michno *et al.* 2019). Frozen tissue sections were thawed and dried under vacuum for 15 min. A series of sequential washes of 100% EtOH (60 s), 70% EtOH (30 s), Carnoy's fluid (6:3:1 EtOH/$CHCl_3$/acetic acid) (90 s), 100% EtOH (15 s), $H_2O$ with 0.2% TFA (60 s), and 100% EtOH (15 s) was carried out. Tissues were subjected to formic acid vapor for 20 min. A mixture of 2,5-dihydroxyacetophenone (2,5-DHAP) and 2,3,4,5,6-pentafluoroacetophenone (PFAP) was used as matrix compound and applied using a HTX TM-Sprayer (HTX Technologies LLC, Carrboro, NC, USA). A matrix solution of 5.7 µl/ml of PFAP and 9.1 mg/ml of DHAP in in 70% ACN(aq), 2% acetic acid / 2% TFA was sprayed onto the tissue sections using the following instrumental parameters: nitrogen flow (10 PSI), spray temperature (75°C), nozzle height (40 mm), eight passes with offsets and rotations, and spray velocity (1000 mm/min), and isocratic flow of 100 µl/min using 70% ACN as pushing solvent.

**MALDI MS imaging**

MALDI-MSI experiments were performed on a rapifleX MALDI-TOF instrument (Bruker Daltonics) using the FlexImaging (v5.0, Bruker Daltonics). Measurements were performed at 10µm spatial resolution, at a laser pulse frequency of 10 kHz with 200 shots collected per pixel. Data were acquired in linear positive mode in the mass range of 1500–6000 Da (mass resolution: m/Δm=1000 (FWHM) at m/z 4515). Pre-acquisition calibration of the system was performed using a combination of peptide calibration standard II and protein calibration standard I, in order to ensure calibration over the entire range of potential Aβ species.

**Data Processing and Image Analysis**

LCO+/PHF+ and LCO+/PHF- plaques were identified from the tile scan images obtained from the IF microscopy. These plaques were identified across the whole tissue sections (approximately $1cm^2$) for each patient involved in the study. These tile scans were overlayed and aligned onto single ion images obtained from MALDI MSI on the sequential tissue section. The IF microscopy signatures were used to guide annotation of single

plaques in the MALDI MSI data as regions of interest (ROI) for further statistical analysis of mass spectrometry peak data using FlexImaging (v5.0, Bruker Daltonics). MS peak data from N=5-10 ROIs (plaques per subtype) across n=3 patient samples were exported as *.CSV files and imported into Origin (version 8.1 OriginLab, Northampton, MA). Bin borders were generated using the PeakAnalyser function in Origin. Peak bin area values were obtained using an in-house developed R script as described previously (Hanrieder et al., 2011). All the data were compiled, and log normalized in Excel.

Average peak data from the different plaque-ROI were analyzed by grouped, univariate statistical comparisons of the respective plaque subtypes (PHF+/PHF-) across patients by means of paired t-statistics ($p<0.05$) using Prism (v.9, GraphPad, San Diego, CA, USA).

## RESULTS

### 1. PHF-1 and RTN3 delineate neuritic plaque pathology

We devised a correlative multimodal plaque imaging paradigm (Figure 1), where IF signatures obtained from one section guide MALDI plaque analysis of Aβ signatures on the facing surface of the consecutive section. On section 1, plaques were stained with fluorescent amyloid probe LCO (Nyström *et al.* 2017) along with markers of neuritic plaques (PHF-1) and dystrophic neurites (RTN3). This was followed by MALDI MSI on the consecutive section and yielded a total of 7-10 plaques per subtype (PHF+ and PHF-) and patient that could be delineated with both correlative imaging techniques.

**[Figure 1]**

In accordance with previous reports on PHF-1 staining of neuritic plaques, we observed LCO+/PHF+ (neuritic) and LCO+/PHF- (non-neuritic) plaques. (Figure 2A, BI-III). (Hu et al., 2007). Similarly, all the LCO+/PHF+ plaques observed in our study were also found to be associated with RTN3+ dystrophic neurites, while all LCO+/PHF- showed no presence of RINDs (Figure 2A, B IV).

**[Figure 2]**

**2. IHC guided MALDI MSI identifies Aβ signatures of neuritic plaques**

To explore the amyloid signatures of neuritic plaques we performed MALDI imaging on the corresponding mirror section. The aim was to analyze the same population of the plaques identified in the immunostaining on the mirror section. Using IF microscopy, LCO+/PHF+ and LCO+/PHF- plaques were outlined across entire cortical brain tissue sections (approximately $1cm^2$) from each patient involved in the study. The IF (LCO/PHF) signatures were co-registered with the MALDI MSI data to guide the annotation of plaques into neuritic (LCO+/PHF+) or non neuritic (LCO+/PHF-). A total of 44 plaques (22 neuritic, 22 non-neuritic, cored) were annotated across three patient samples. MALDI MSI signature from the PHF+/- plaque populations were extracted, binned and statistically analyzed for differences in Aβ content (Table 2). Across all detected Aβ species, Aβ1-42(ox) (m/z 4528) and Aβ2-42 (m/z 4398) were found to be significantly higher in neuritic (LCO+/PHF+) than in non neuritic, cored plaques (LCO+/PHF-) (Figure 3).

**[Figure 3]**

**3. Aβ peptide patterns in neuritic plaques correlate with plaque associated dystrophic neurites**

To validate the neuritic identity of NP we used both PHF and RTN3 to outline NPs in situ. While the first aim was to classify senile cored plaques into NP and non-NP, we then moved on to investigate whether the neuritic marker's IF intensity correlated with the levels of the different Aβ species within each plaque. Here, Aβ1-42(ox) (R=0.2090, p=0.0282) but not Aβ 2-42showed a significant correlation with RTN3 (intensity/$\mu m^2$) IF. In contrast no positive correlation was observed for any of the Aβ peptides with PHF.

**DISCUSSION**

Amyloid plaques show a variety of morphologies, described historically as diffuse, cored, neuritic, compact, fibrillar, and others. They vary from each other in terms of their maturity of fibrils, density of the accumulated fibrils and in some cases their composition. The presence of these plaques in the brain is the source of immunogenic stimuli in the

surrounding neurons and glia. This alteration in the homeostasis of the brain regions could trigger dystrophy in neurons present in the microenvironment around the plaques.

The characterization of senile plaques in postmortem brain tissue has for decades relied on histochemical, immunohistochemical, or immunofluorescent detection. This approach has two significant limitations with respect to specificity and the ability for comprehensive spatial detection of multiple truncated Aβ isoforms. We and others have previously demonstrated MALDI MSI to be a powerful tool to delineate Aβ peptide *in situ* on the single plaque level (Michno et al., 2019a, Carlred et al., 2016, Kakuda et al., 2017). One challenge however remains with respect to integrating MALDI MSI with IHC towards larger, protein markers that cannot be detected with MALDI such as RTN3 or Tau. Acquisition of fluorescent microscopy and MALDI MSI of peptides from the same tissue section is challenging due to laser distortion effects impeding subsequent immunolabeling and fluorescent imaging (Kaya et al., 2017).

In this first of its kind work, we employed a correlative chemical imaging approach to identify Aβ signatures associated with different populations of plaques, specifically neuritic plaques. We have previously shown that cored plaques show distinct signatures compared to diffuse plaques, which can be delineated morphologically using structure sensitive probes that can be integrated in the MALDI MSI analysis from the same tissue. However, to delineate non-diffuse plaques, i.e., mature/cored plaques including neuritic plaques, IHC based plaque classification is necessary. We employed a methodology that involves the novel combination of correlative mass spectrometry imaging and fluorescent microscopy, where we used PHF-1 antibody as a marker to differentiate neuritic plaques from non-neuritic deposits. For fluorescence microscopy on human brain sections, an autofluorescence quenching agents – Trueblack$^{TM}$ was used to neutralise the autofluorescence of lipofuscin. Also, secondary antibodies like Alexafluor 594 (emission peaks at around 614 nm) and Alexafluor 647(emission peaks at around 670 nm) which are infra-red and far-red–fluorescent dyes respectively are used to avoid overlap with the spectral emission range of lipofuscin (540-570nm).

Fluorescent microscopy-based immunofluorescence and LCO staining allowed us to classify plaque types and guided MALDI MSI analyses to identify differences in Aβ patterns.



Brain Connectivity
Correlative chemical imaging identifies amyloid peptide signatures of neuritic plaques and dystrophy in human sporadic Alzheimer's disease (DOI: 10.1089/brain.2022.0047)
This paper has been peer-reviewed and accepted for publication, but has yet to undergo copyediting and proof correction. The final published version may differ from this proof.

With this approach, we observed that neuritic (LCO+/PHF+) were characterized by increased levels of Aβ1-42(ox) and Aβ2-42 as compared to non-neritic (LCO+/PHF-) plaques.

Previous studies have shown that compared to diffuse plaques, Th/CR-positive, mature, cored plaques show higher Aβ1-40 levels along with higher levels of AβpE3-42 and AβpE11-42 (Michno et al., 2019a). In the present study Aβ1-40 was not found to be different between neuritic (LCO+/PHF+) and non-neuritic (LCO+/PHF-) plaques. In addition, there were no differences in the N-terminally truncated pyroglutamated forms of Aβx-42 (Aβ3pE-42 and Aβ11pE-42). This suggests that the PHF+ and PHF- status, rather than being related to maturity of a plaque, is a suitable marker of secondary mechanisms that are linked to neuronal pathology and dystrophy. Interestingly, analysis of the MALDI MSI identified Aβ2–42 to be significantly higher in PHF+ plaques as compared to PHF- deposit.

Aβ2–42 has previously been implicated in plaque formation and aggregation dynamics (Wiltfang et al., 2001). Here, N-terminal truncations were found to synergistically increases the aggregation potential of Aβ peptides. This suggests that Aβ2–42 formation may serve as one of the initial factors for seeding aggregation preceding the formation of plaque core β-amyloid. This would also accelerate the aggregation kinetics of the fibrils, leading to increased amyloid deposition and aggregation, respectively. In line with these findings, Bibl *et al* reported low levels Aβ2-42 in AD CSF compared to non-demented controls and FTD (Bibl et al., 2012). Interestingly, CSF Aβ2-42 was diagnostically a stronger indicator of AD than Aβ1-40/1-42, which suggests that indeed Aβ2-42 might detect neurodegeneration associated amyloid plaques pathology, i.e., neuritic plaques rather than general plaque load as indicated by Aβ1-40/1-42.

Another finding of our work was that Aβ1-42ox was increased in neuritic plaques compared to other non-neuritic, plaques and suggests involvement of oxidative stress on neuritic plaque pathology. Further, Aβ1-42(ox) was observed to correlate with neuritic plaque associated dystrophy as indicated by RTN3 immunolabelling.



Brain Connectivity
Correlative chemical imaging identifies amyloid peptide signatures of neuritic plaques and dystrophy in human sporadic Alzheimer's disease (DOI: 10.1089/brain.2022.0047)
This paper has been peer-reviewed and accepted for publication, but has yet to undergo copyediting and proof correction. The final published version may differ from this proof.

This is relevant as oxidative stress has been identified a key mechanism upon which amyloid may exert its pathogenicity. Specifically, amyloid pathogenicity was suggested to involve intracellular disturbance of mitochondrial function leading to generation of reactive oxygen species and subsequent intraneuronal cytotoxic mechanism that eventually leads to neuronal cell death (Cheignon et al., 2018). Specifically, Aβ1-42 has been shown to induce oxidative stress, catalyzing the formation of reactive oxygen species and downstream neurotoxic processes including conformational changes and oxidation of membrane proteins as well as lipid peroxidation (Butterfield and Boyd-Kimball, 2018) (Ko et al., 2015)(Yan et al., 1994). Importantly, Aβ induced generation of reactive oxygen species and oxidative stress, respectively, has been demonstrated to affect neuronal processes and result in structural changes in DN that are associated with NPs (Garcia-Alloza et al., 2006).

Further, a prolonged exposure of neurons to Aβ was found to induce ER stress and ER stress mediated autophagy, respectively that triggers caspase mediated apoptotic pathways (Nakagawa et al., 2000, Costa et al., 2012). Previous reports demonstrated a surge in RTN3 expression with increase in ER stress as an anti-apoptotic response (Wan et al., 2007). Hence, elevated RTN3 levels in neuritic plaques and the correlation of RIND with Aβ1-42ox point towards Aβ induced ER stress and oxidative stress, including ROS mediated ER stress that affect neuroal processes abd ultimately result DN formation.

Dystrophic neurites are swollen, dysfunctional pre-synaptic terminals that are found across and around neuritic plaques. DN can be found in different forms including axonal dystrophy, which is the prominent kind of dystrophy observed for neurons. DNs are indicative of pathological processes including altered axonal transport (Shi et al., 2009) and cytoskeletal changes (Dickson et al., 1999). Such axonal alterations would result in axonal dystrophy which has been associated with the presence of amyloid plaques. As hypothesized by Shi et al, prolonged deposition of amyloid deposits results in the microtubule disruption and changes associated with autophagy (Shi et al., 2009). This can result in the accumulation of one of the autophagy associated proteins like RTN3, and axonal swelling in the neurons present around the amyloid deposition. Increase in the amyloid deposition increases the size of the plaques, thus bringing a greater number of

surrounding neuronal processes in contact of the plaques, contributing to increased number of dystrophies.

Interestingly, increased expression of RTN3 in the regions of the marked plaques indicates axonal dystrophy prevailing in the axons of neurons. The here observed correlation of RTN3 with one of the Aβ species (Aβ1-42(ox)) that were which increased in NPs, further adds to the notion that axonal dystrophy is one of the characteristic feature of neuritic plaque pathology (Shi et al., 2009)(Dickson et al., 1999)(Oakley et al., 2006, Sharoar et al., 2019).

## CONCLUSIONS

The present study represents the first of its kind to delineate the biochemical characteristics of neuritic Aβ plaque pathology using advanced correlative immunostaining guided mass spectrometry imaging. The results show that neuritic plaques are chemically different from other cored, plaque deposits with respect to their Aβ truncation and modification pattern. The here identified Aβ signatures delineate neuritic plaques from other plaques as well as display association with dystrophy. This information is difficult to obtain with conventional biochemical imaging techniques and highlight the emerging role of MS imaging in biomedical research. Together, these correlative imaging data shed light on the complex biochemical architecture of neuritic plaques and associated dystrophic neurites. The molecular traits associated with neuritic plaque pathology in turn are obvious targets for disease-modifying treatments, as well as potential novel biomarkers of Aβ pathogenicity.

## AUTHOR INFORMATION

* Corresponding Author

Email: jh@gu.se; Phone: (+46)702571888



Brain Connectivity
Correlative chemical imaging identifies amyloid peptide signatures of neuritic plaques and dystrophy in human sporadic Alzheimer's disease (DOI: 10.1089/brain.2022.0047)
This paper has been peer-reviewed and accepted for publication, but has yet to undergo copyediting and proof correction. The final published version may differ from this proof.

ORCID

Jörg Hanrieder, 0000-0001-6059-198X

Wojciech Michno: 0000-0002-3096-3604

Henrik Zetterberg: 0000-0003-3930-4354

**Author contribution:**

JH conceived and designed the study. TL selected the cases from QSBB archives. SK, JG, DJ performed experiments. KS, JG, WM, KB, TL, HZ and JH analyzed and discussed the data. KS, WM and JH wrote the manuscript.

**ACKNOWLEDGEMENTS**

We thank the staff at Centre for Cellular Imaging (CCI), Core Facilities, The Sahlgrenska Academy, University of Gothenburg, for help with development of the hyperspectral imaging paradigm and microscopy expertise. The Queen Square Brain Bank is supported by the Reta Lila Weston Institute of Neurological Studies, UCL Queen Square Institute of Neurology.

**Funding**

JH is supported by the Swedish Research Council VR (#2018-02181 and #2019-02397), the Swedish Alzheimer Foundation (#AF-968238, #AF-939767) and Åhlén-Stiftelsen. (#213027). Stiftelsen Gamla Tjänarinnor (SK, JH, WM, HZ, KB), Gun och Bertil Stohnes Stiftelse (JH, SK, WM) are achnowledged for financial support. WM is supported on a Postddoc grant from the Knut and Alice Wallenberg Foundation, HZ is a Wallenberg Scholar supported by grants from the Swedish Research Council (#2018-02532 and #2019-02397), the European Research Council (#681712 and #101053962), Swedish State Support for Clinical Research (#ALFGBG-71320), the Alzheimer Drug Discovery Foundation (ADDF), USA (#201809-2016862), the AD Strategic Fund and the Alzheimer's Association (#ADSF-21-831376-C, #ADSF-21-831381-C and #ADSF-21-831377-C), the Olav Thon Foundation, the Erling-Persson Family Foundation, Hjärnfonden, Sweden (#FO2019-0228), the European Union's Horizon 2020 research and innovation programme under the Marie Skłodowska-Curie grant agreement No 860197 (MIRIADE), the European Union Joint Programme –

Neurodegenerative Disease Research (JPND2021-00694), and the UK Dementia Research Institute at UCL (UKDRI-1003). KB is supported by the Swedish Research Council (#2017-00915), the Alzheimer Drug Discovery Foundation (ADDF), USA (#RDAPB-201809-2016615), the Swedish Alzheimer Foundation (#AF-930351, #AF-939721 and #AF-968270), Hjärnfonden, Sweden (#FO2017-0243 and #ALZ2022-0006), the Swedish state under the agreement between the Swedish government and the County Councils, the ALF-agreement (#ALFGBG-715986 and #ALFGBG-965240), the European Union Joint Program for Neurodegenerative Disorders (JPND2019-466-236), the National Institute of Health (NIH), USA, (grant #1R01AG068398-01), and the Alzheimer's Association 2021 Zenith Award (ZEN-21-848495). TL is supported by an Alzheimer's Research UK senior fellowship. Queen Square Brain Bank is supported by the Reta Lila Weston Institute for Neurological Studies.

**Conflicts of interest**

HZ has served at scientific advisory boards and/or as a consultant for Abbvie, Alector, ALZPath, Annexon, Apellis, Artery Therapeutics, AZTherapies, CogRx, Denali, Eisai, Nervgen, Novo Nordisk, Pinteon Therapeutics, Red Abbey Labs, reMYND, Passage Bio, Roche, Samumed, Siemens Healthineers, Triplet Therapeutics, and Wave, has given lectures in symposia sponsored by Cellectricon, Fujirebio, Alzecure, Biogen, and Roche, and is a co-founder of Brain Biomarker Solutions in Gothenburg AB (BBS), which is a part of the GU Ventures Incubator Program (outside submitted work). KB has served as a consultant, at advisory boards, or at data monitoring committees for Abcam, Axon, BioArctic, Biogen, JOMDD/Shimadzu. Julius Clinical, Lilly, MagQu, Novartis, Ono Pharma, Pharmatrophix, Prothena, Roche Diagnostics, and Siemens Healthineers, and is a co-founder of Brain Biomarker Solutions in Gothenburg AB (BBS), which is a part of the GU Ventures Incubator Program, outside the work presented in this paper.

**REFERENCES**

Bayer, TA. Pyroglutamate Abeta cascade as drug target in Alzheimer's disease. Mol Psychiatry 2022;27(4):1880-1885;10.1038/s41380-021-01409-2

Bibl, M, Gallus, M, Welge, V, et al. Cerebrospinal fluid amyloid-β 2-42 is decreased in Alzheimer's, but not in frontotemporal dementia. J Neural Transm (Vienna) 2012;119(7):805-813;10.1007/s00702-012-0801-3

Braak, H Braak, E. Neuropathological stageing of Alzheimer-related changes. Acta neuropathologica 1991;82(4):239-259;

Butterfield, DA Boyd-Kimball, D. Oxidative Stress, Amyloid-β Peptide, and Altered Key Molecular Pathways in the Pathogenesis and Progression of Alzheimer's Disease. J Alzheimers Dis 2018;62(3):1345-1367;10.3233/jad-170543

Carlred, L, Michno, W, Kaya, I, et al. Probing amyloid-beta pathology in transgenic Alzheimer's disease (tgArcSwe) mice using MALDI imaging mass spectrometry. J Neurochem 2016;138(3):469-478;10.1111/jnc.13645

Cheignon, C, Tomas, M, Bonnefont-Rousselot, D, et al. Oxidative stress and the amyloid beta peptide in Alzheimer's disease. Redox Biol 2018;14(450-464;10.1016/j.redox.2017.10.014

Costa, RO, Ferreiro, E, Martins, I, et al. Amyloid β-induced ER stress is enhanced under mitochondrial dysfunction conditions. Neurobiol Aging 2012;33(4):824.e825-816;10.1016/j.neurobiolaging.2011.04.011

Dickson, TC, King, CE, Mccormack, GH, et al. Neurochemical diversity of dystrophic neurites in the early and late stages of Alzheimer's disease. Exp Neurol 1999;156(1):100-110;10.1006/exnr.1998.7010

Dickson, TC Vickers, JC. The morphological phenotype of beta-amyloid plaques and associated neuritic changes in Alzheimer's disease. Neuroscience 2001;105(1):99-107;10.1016/s0306-4522(01)00169-5

Garcia-Alloza, M, Dodwell, SA, Meyer-Luehmann, M, et al. Plaque-derived oxidative stress mediates distorted neurite trajectories in the Alzheimer mouse model. J Neuropathol Exp Neurol 2006;65(11):1082-1089;10.1097/01.jnen.0000240468.12543.af

Grumati, P, Morozzi, G, Holper, S, et al. Full length RTN3 regulates turnover of tubular endoplasmic reticulum via selective autophagy. Elife 2017;6(10.7554/eLife.25555

Hanrieder, J, Ljungdahl, A, Falth, M, et al. L-DOPA-induced dyskinesia is associated with regional increase of striatal dynorphin peptides as elucidated by imaging mass spectrometry. Molecular & cellular proteomics : MCP 2011;10(10):M111.009308;10.1074/mcp.M111.009308

Hu, X, Shi, Q, Zhou, X, et al. Transgenic mice overexpressing reticulon 3 develop neuritic abnormalities. EMBO J 2007;26(11):2755-2767;10.1038/sj.emboj.7601707

Kakuda, N, Miyasaka, T, Iwasaki, N, et al. Distinct deposition of amyloid-beta species in brains with Alzheimer's disease pathology visualized with MALDI imaging mass spectrometry. Acta Neuropathol Commun 2017;5(1):73;10.1186/s40478-017-0477-x

Kaya, I, Michno, W, Brinet, D, et al. Histology-Compatible MALDI Mass Spectrometry Based Imaging of Neuronal Lipids for Subsequent Immunofluorescent Staining. Anal Chem 2017;89(8):4685-4694;10.1021/acs.analchem.7b00313

Kirmess, KM, Meyer, MR, Holubasch, MS, et al. The PrecivityAD test: Accurate and reliable LC-MS/MS assays for quantifying plasma amyloid beta 40 and 42 and apolipoprotein E proteotype for the assessment of brain amyloidosis. Clin Chim Acta 2021;519(267-275;10.1016/j.cca.2021.05.011

Ko, SY, Ko, HA, Chu, KH, et al. The Possible Mechanism of Advanced Glycation End Products (AGEs) for Alzheimer's Disease. PLoS One 2015;10(11):e0143345;10.1371/journal.pone.0143345

Lenders, MB, Peers, MC, Tramu, G, et al. Dystrophic neuropeptidergic neurites in senile plaques of Alzheimer's disease precede formation of paired helical filaments. Acta Neurol Belg 1989;89(3-4):279-285;

Matthews, KA, Xu, W, Gaglioti, AH, et al. Racial and ethnic estimates of Alzheimer's disease and related dementias in the United States (2015-2060) in adults aged ≥65 years. Alzheimers Dement 2019;15(1):17-24;10.1016/j.jalz.2018.06.3063

Michno, W, Nystrom, S, Wehrli, P, et al. Pyroglutamation of amyloid-betax-42 (Abetax-42) followed by Abeta1-40 deposition underlies plaque polymorphism in progressing Alzheimer's disease pathology. The Journal of biological chemistry 2019a;294(17):6719-6732;10.1074/jbc.RA118.006604

Michno, W, Stringer, KM, Enzlein, T, et al. Following spatial Aβ aggregation dynamics in evolving Alzheimer's disease pathology by imaging stable isotope labeling kinetics. Science Advances 2021;7(25):eabg4855;10.1126/sciadv.abg4855

Michno, W, Wehrli, P, Meier, SR, et al. Chemical imaging of evolving amyloid plaque pathology and associated Aβ peptide aggregation in a transgenic mouse model of Alzheimer's disease. J Neurochem 2020;152(5):602-616;10.1111/jnc.14888

Michno, W, Wehrli, PM, Blennow, K, et al. Molecular imaging mass spectrometry for probing protein dynamics in neurodegenerative disease pathology. J Neurochem 2019b;151(4):488-506;10.1111/jnc.14559

Moloney, CM, Lowe, VJ Murray, ME. Visualization of neurofibrillary tangle maturity in Alzheimer's disease: A clinicopathologic perspective for biomarker research. Alzheimers Dement 2021;17(9):1554-1574;10.1002/alz.12321

Montine, TJ, Phelps, CH, Beach, TG, et al. National Institute on Aging-Alzheimer's Association guidelines for the neuropathologic assessment of Alzheimer's disease: a practical approach. Acta neuropathologica 2012;123(1):1-11;10.1007/s00401-011-0910-3

Nakagawa, T, Zhu, H, Morishima, N, et al. Caspase-12 mediates endoplasmic-reticulum-specific apoptosis and cytotoxicity by amyloid-beta. Nature 2000;403(6765):98-103;10.1038/47513

Oakley, H, Cole, SL, Logan, S, et al. Intraneuronal beta-amyloid aggregates, neurodegeneration, and neuron loss in transgenic mice with five familial Alzheimer's disease mutations: potential factors in amyloid plaque formation. J Neurosci 2006;26(40):10129-10140;10.1523/JNEUROSCI.1202-06.2006

Otvos, L, Jr., Feiner, L, Lang, E, et al. Monoclonal antibody PHF-1 recognizes tau protein phosphorylated at serine residues 396 and 404. J Neurosci Res 1994;39(6):669-673;10.1002/jnr.490390607

Selkoe, DJ. Alzheimer's disease is a synaptic failure. Science 2002;298(5594):789-791;10.1126/science.1074069

Sevigny, J, Chiao, P, Bussiere, T, et al. The antibody aducanumab reduces Abeta plaques in Alzheimer's disease. Nature 2016;537(7618):50-56;10.1038/nature19323

Sharoar, MG, Hu, X, Ma, XM, et al. Sequential formation of different layers of dystrophic neurites in Alzheimer's brains. Mol Psychiatry 2019;24(9):1369-1382;10.1038/s41380-019-0396-2

Shi, Q, Hu, X, Prior, M, et al. The occurrence of aging-dependent reticulon 3 immunoreactive dystrophic neurites decreases cognitive function. J Neurosci 2009;29(16):5108-5115;10.1523/JNEUROSCI.5887-08.2009

Swanson, CJ, Zhang, Y, Dhadda, S, et al. A randomized, double-blind, phase 2b proof-of-concept clinical trial in early Alzheimer's disease with lecanemab, an anti-Abeta protofibril antibody. Alzheimers Res Ther 2021;13(1):80;10.1186/s13195-021-00813-8

Wan, Q, Kuang, E, Dong, W, et al. Reticulon 3 mediates Bcl-2 accumulation in mitochondria in response to endoplasmic reticulum stress. Apoptosis 2007;12(2):319-328;10.1007/s10495-006-0574-y

Wiltfang, J, Esselmann, H, Cupers, P, et al. Elevation of beta-amyloid peptide 2-42 in sporadic and familial Alzheimer's disease and its generation in PS1 knockout cells. The Journal of biological chemistry 2001;276(46):42645-42657;10.1074/jbc.M102790200

Yan, SD, Chen, X, Schmidt, AM, et al. Glycated tau protein in Alzheimer disease: a mechanism for induction of oxidant stress. Proc Natl Acad Sci U S A 1994;91(16):7787-7791;10.1073/pnas.91.16.7787

Brain Connectivity

Correlative chemical imaging identifies amyloid peptide signatures of neuritic plaques and dystrophy in human sporadic Alzheimer's disease (DOI: 10.1089/brain.2022.0047)



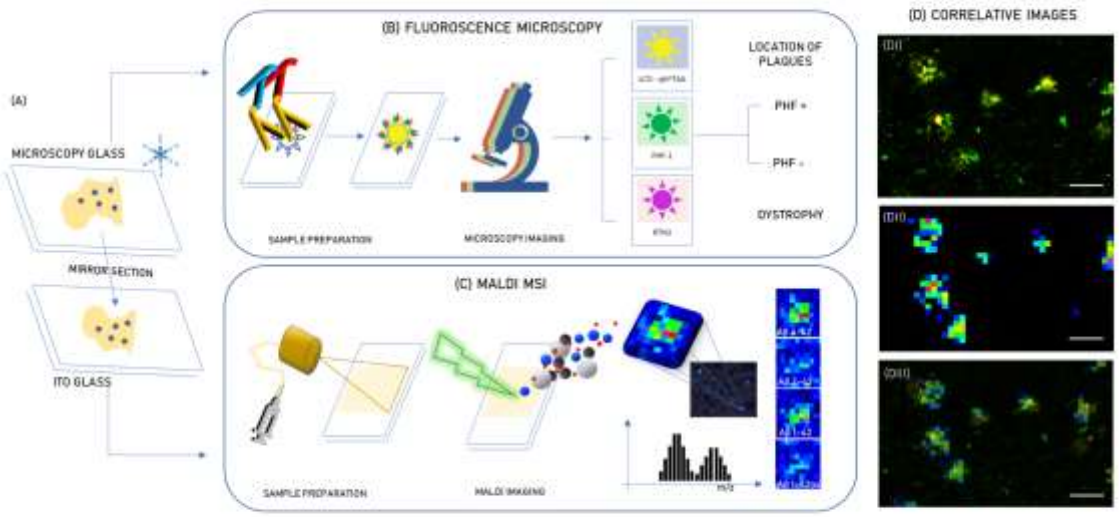


**Figure 1. Correlative Imaging of senile plaques. (A)** Consecutive brain sections are collected in mirror format onto both frosted (for light microscopy) and ITO-coated glasses (for MALDI MSI), **(B)**. Sections on frosted glass are stained with IHC and LCO probes for visualizing various plaque types and **(C)** MALDI MSI is performed on ITO-coated glasses**(D)** IF-LCO images guides the annotation of plaque ROI in the MALDI image. **(DI)** Microscopy image with plaques **(DII)** Single peptide image obtained from MALDI MSI **(DIII)** Overlay of light microscopy image and MALDI MSI single peptide image.

Brain Connectivity
Correlative chemical imaging identifies amyloid peptide signatures of neuritic plaques and dystrophy in human sporadic Alzheimer's disease (DOI: 10.1089/brain.2022.0047)



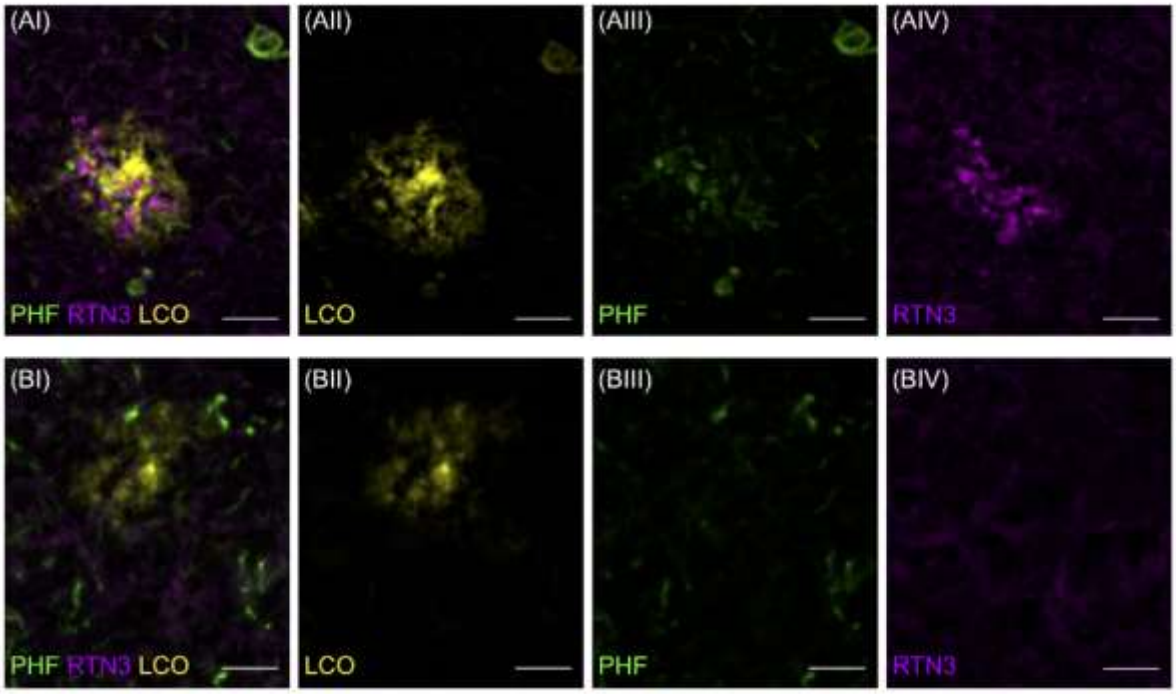


**Figure 2. Immunohistochemistry of PHF+ and PHF- plaques and quantification of RTN3. (AI and BI)** Overlay image of three channel (assigned pseudo colors) respectively comprising of **(AII, BII)** LCO in yellow **(AIII, BIII)** PHF and **(AIV, BIV)** RTN3 (Scale = 20µm)

Brain Connectivity
Correlative chemical imaging identifies amyloid peptide signatures of neuritic plaques and dystrophy in human sporadic Alzheimer's disease (DOI: 10.1089/brain.2022.0047)



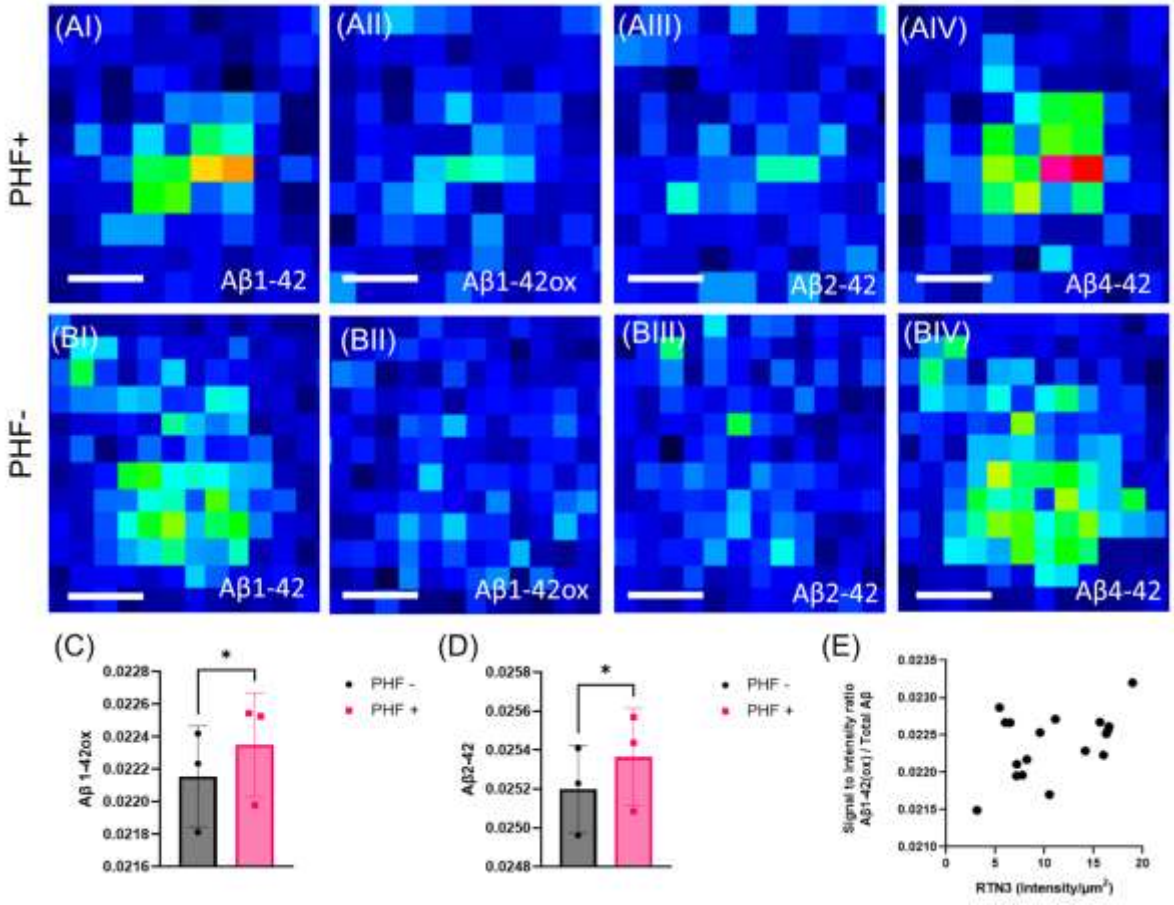


**Figure 3. MALDI Imaging of amyloid plaques. (A,B) Single ion images of** Aβ peptides in PHF+ (A) and PHF- (B) plaques. **(C)** Bar plots Aβ1-42ox **(D)** and Aβ2-42 that were both higher in PHF+ plaques than in PHF- plaques. **(C)** Correlation of Aβ1-42ox with RTN3 (p=0.0282) *significance is shown as $p < 0.05$.

**TABLES**

**Table 1:** Demographic data: AAO: Age at onset; AAD: Age at death, CERAD: Consortium to Establish a Registry for Alzheimer's Disease; ABC is a combined score based on Thal phase, Braak stage, and CERAD score; PCA: Posterior cortical atrophy; PMD: Post mortem delay

| **Patient ID** | **AAO** | **AAD** | **Gender** | **Clinical Diagn.** | **Pathol. Diagn.** | **Braak** | **Thal** | **CERAD** | **ABC** | **PMD (h:m)** |
|---|---|---|---|---|---|---|---|---|---|---|
| sAD1 | 43 | 58 | F | AD | AD | VI | 5 | 2 | A3B3C2 | 58:50 |
| sAD2 | 54 | 65 | M | AD | AD | VI | 5 | 3 | A3B3C3 | 34:25 |
| sAD3 | 58 | 68 | M | PCA | AD | VI | 5 | 3 | A3B3C3 | 52:05 |



Brain Connectivity
Correlative chemical imaging identifies amyloid peptide signatures of neuritic plaques and dystrophy in human sporadic Alzheimer's disease (DOI: 10.1089/brain.2022.0047)

**Table 2:** Masses of the detected Aβ isoforms.

| Peptide | $[M+H]^+$ | $[M+H]^+$ avg. | Peptide Sequence |
|---|---|---|---|
| Aβ11pE-42 | 3132.444 | 3132.433 | DAEFRHDSGYEVHHQKLVFFAEDVGSN |
| Aβ1-29 | 3317.557 | 3317.549 | DAEFRHDSGYEVHHQKLVFFAEDVGSNKG |
| Aβ7-42 | 3759,5 | 3759,5 | DSGYEVHHQKLVFFAEDVGSNKGAIIGLMVGGVVIA |
| Aβ2-36 | 3899.9416 | 3902,949 | AEFRHDSGYEVHHQKLVFFAEDVGSNKGAIIGLMV |
| Aβ2-38 | 4014.983 | 4014,5 | AEFRHDSGYEVHHQKLVFFAEDVGSNKGAIIGLMVGG |
| Aβ1-37 | 4071.989 | 4071.99 | DAEFRHDSGYEVHHQKLVFFAEDVGSNKGAIIGLMVG |
| Aβ1-38 | 4130.01 | 4128 | DAEFRHDSGYEVHHQKLVFFAEDVGSNKGAIIGLMVGG |
| Aβ5-43 | 4151,14948 | 4154 | RHDSGYEVHHQKLVFFAEDVGSNKGAIIGLMVGGVVIAT |
| Aβ4-42 | 4198 | 4199,5 | FRHDSGYEVHHQKLVFFAEDVGSNKGAIIGLMVGGVVIA |
| Aβ3pE-42 | 4308.2 | 4311 | pEFRHDSGYEVHHQKLVFFAEDVGSNKGAIIGLMVGGVVIA |
| Aβ1-40 | 4328.149 | 4329,5 | DAEFRHDSGYEVHHQKLVFFAEDVGSNKGAIIGLMVGGVV |
| Aβ2-42 | 4398 | 4400 | AEFRHDSGYEVHHQKLVFFAEDVGSNKGAIIGLMVGGVVIA |
| Aβ1-42 | 4512.275 | 4515,5 | DAEFRHDSGYEVHHQKLVFFAEDVGSNKGAIIGLMVGGVVIA |
| Aβ1-42(ox) | 4528.275 | 4531,5 | DAEFRHDSGYEVHHQKLVFFAEDVGSNKGAIIGLMVGGVVIA + oxidation |



Brain Connectivity
Correlative chemical imaging identifies amyloid peptide signatures of neuritic plaques and dystrophy in human sporadic Alzheimer's disease (DOI: 10.1089/brain.2022.0047)